The Influences of Carbon and Molybdenum on the Progress of Liquid Phase Sintering and the Microstructure of Boron-Containing Powder Metallurgy Steel

MING-WEI WU

Boron is an optimal alloying element for liquid phase sintering (LPS) of powder metallurgy (PM) Fe-based materials. However, the influences of various alloying elements on the progress of LPS are still undetermined. The aim of this study was to clarify the effects of carbon and molybdenum on the LPS and microstructure of boron-containing PM steel. The results showed that adding 0.5 wt pct C and 1.5 wt pct Mo, and particularly the former, promotes the LPS and increases the sintered density. With the addition of 0.5 wt pct C, liquid can be generated in two distinct regions, and the secondary liquid improves the densification. After 1523 K (1250 °C) sintering, the increases in sintered densities of Fe-0.4B, Fe-0.4B-1.5Mo, Fe-0.4B-0.5C, and Fe-0.4B-1.5Mo-0.5C steels were 0.33, 0.47, 0.56, and 0.64 g/cm^3, respectively. Thermodynamic simulation also demonstrated that the increases in sintered densities were correlated with the liquid volumes formed at 1523 K (1250 °C). In conclusion, adding 0.5 wt pct C to B-containing PM steels facilitates the formation of a secondary liquid phase and higher liquid volume, resulting in better densification.

DOI: 10.1007/s11661-014-2619-0

I. INTRODUCTION

POWDER metallurgy (PM) steels are widely used in automobile and mechanical parts. Their mechanical properties, including the hardness, tensile strength, impact resistance, and fatigue properties, can be increased by adequate processing parameters and alloy designs.[1–7] Reducing the amount of alloying elements is also a promising direction for the future development of PM steels.[8,9] However, the mechanical properties of PM steels are lower than those of wrought steels due to their porosity, which ranges from 5 to 15 vol pct. Increasing the sintered density using novel compaction techniques, such as warm compaction (WC), double-pressing/double-sintering (DPDS), and high velocity compaction (HVC), is a versatile means to increase not only the sintered density but also the various mechanical properties.[10–13] Unfortunately, these compaction techniques incur additional production costs.

Liquid phase sintering (LPS), which involves adding boron,[14–27] copper,[28,29] and phosphorous,[30,31] particularly boron, is also an effective method of increasing the sintered density of PM steels. In wrought steels, boron is mainly used to increase the hardenability. With as little as 0.002 wt pct B, the hardenability of wrought steels can be obviously increased.[32,33] However, in PM steels, boron is mostly used as an alloying element for promoting sintering densification by LPS. Adding boron can result in a eutectic reaction (Fe + $Fe_2B \rightarrow L$) and effectively improve the sintered density.[14–18] The effects of boron in the LPS of alloy steels,[14–23] stainless steels,[24] maraging steels,[25] and high-Cr steels[26,27] have been extensively studied.

Among the material compositions investigated in the literature, Fe-B[14–18] and Fe-B-Mo[14–20] are two major systems that have received much focus. Molybdenum is an important alloying element in PM alloy steels due mainly to its high hardenability and low oxygen affinity. German *et al.*[14] indicated that at a given boron content, the amount of liquid is decreased by increasing molybdenum content because molybdenum can react with boron to form $FeMoB_2$ compound and decrease the amount of liquid phase for densification. Dudrová *et al.*[15] found that the LPS densification of Fe-B-Mo steel is higher than that of Fe-B steel, though a lower amount of liquid phase is formed in the Fe-B-Mo steel. Selecká *et al.*[16] also showed that the increase in density after LPS of Fe-0.4B is greater when the molybdenum content is increased from 0 to 1.5 wt pct. Sarasola *et al.*[17,18] studied the influence of molybdenum content on LPS of Fe-0.3B-xMo steels (x = 0, 0.5, 1.5, 3.5) and found that the liquid phase is generated at 1448 K (1175 °C) in steels with molybdenum content lower than 1.5 wt pct. However, in Fe-0.3B-3.5Mo steel, the eutectic reaction is inhibited, so the liquid phase can be formed only at temperatures higher than 1473 K (1200 °C). The above findings clearly demonstrate the importance and complexity of molybdenum in the LPS of various PM steels.

The effects of carbon on the LPS of B-containing PM steels have been also investigated in several

MING-WEI WU, Associate Professor, is with the Department of Materials and Mineral Resources Engineering, National Taipei University of Technology, No. 1, Sec. 3, Zhong-Xiao E. Rd., Taipei 10608, Taiwan, ROC. Contact e-mail: mwwu@ntut.edu.tw, r91527045@ntu.edu.tw
Manuscript submitted May 26, 2014.
Article published online October 16, 2014

studies.[16,21–23,25] Xiu *et al.*[23] indicated that in Fe-B-Mo-C steel, increasing the carbon content from 0.2 to 0.44 wt pct raised the sintered density, total shrinkage, and maximum shrinkage rate. On the other hand, Liu *et al.*[22] showed that the influence of carbon is negligible on LPS densification of Fe-0.3B-1Ni-1Mo-C steel up to 0.4 wt pct C. To date, the effects of carbon on LPS of B-containing PM steels have rarely been examined in detail. However, since the role of carbon must be clearly identified because it is an indispensable element in PM alloy steels, the objective of this study was to clarify the influences of carbon and molybdenum on LPS of B-containing PM steel. The progress of LPS, liquid formation and its volume, and the microstructures of Fe-B, Fe-B-Mo, Fe-B-C, and Fe-B-Mo-C steels were examined and are discussed.

II. EXPERIMENTAL PROCEDURE

To identify the effects of carbon and molybdenum on LPS of B-containing PM steels, Fe-0.4B, Fe-0.4B-1.5Mo, Fe-0.4B-0.5C, and Fe-0.4B-1.5Mo-0.5C steels were prepared for this study. The designations of these four steels were FB, FBM, FBC, and FBMC, respectively. The base powders were pure iron powder and Fe-1.5Mo prealloyed powder. These two base powders were admixed with 0.4 wt pct elemental boron powder and 0.75 wt pct ethylene bis-stearamide, which is a lubricant, in a mixer for 60 minutes to homogenize the powder mixture. For the steels with 0.5 wt pct C, 0.6 wt pct graphite powder was also added into the powder mixture. After sintering, the combined carbon content in the steels with carbon was about 0.5 wt pct due to decarburization. The characteristics of the pure iron, Fe-1.5Mo, boron, and graphite powders are listed in Table I. The average sizes of the boron and graphite powders used were about 2 and 9 μm, respectively, according to observations by SEM (JSM-6360, JEOL, Tokyo, Japan). The four powder mixtures were then uniaxially compacted using die compaction at a pressure of 600 MPa into green compact disks that were 13 mm in diameter and 7 mm thick. The green densities of these four steels were divergent because of the differences in powder compressibility. The green densities of FB, FBM, FBC, and FBMC were 7.06, 7.02, 6.92, and 6.87 g/cm^3, respectively.

To remove the lubricant, the green compacts were first heated at 5 K/min to 823 K (550 °C) for 15 minutes. These resulting debound compacts were subsequently heated at 10 k/min to the sintering temperatures 1423 K, 1473 K, and 1523 K (1150 °C, 1200 °C, and 1250 °C) without soaking at the temperature, followed by furnace cooling. The atmosphere used for the debinding and sintering was argon. The sintered densities of the steels sintered at various temperatures were measured using Archimedes method. To observe the microstructure, the sintered steels were ground, polished, and etched with a 2 pct nital and 4 pct picral solution. The metallographic specimens were then examined under OM and SEM. An electron probe micro-analyzer (EPMA, JXA-8200SX, JEOL, Tokyo, Japan) was used to identify the elemental distributions of boron, molybdenum, carbon, and iron in the steels. To clarify the temperature region for liquid formation, the steels were examined by differential scanning calorimetry (DSC, STA 449 F3, NETZSCH, Selb, Germany). Furthermore, Thermo-Calc software coupled with a TCFE3 database (Thermo-Calc Software, Stockholm, Sweden) was used to simulate the liquid volumes of the four steels sintered at 1523 K (1250 °C) to correlate the alloying elements with the densification by LPS.

III. RESULTS AND DISCUSSION

A. *Microstructure*

Figures 1 through 3 show the microstructures of the four steels after they sintered at 1423 K, 1473 K, and 1523 K (1150 °C, 1200 °C, and 1250 °C). Figure 1 indicates that no liquid was generated after 1423 K (1150 °C) sintering in the four steels. The pores were large and irregular, irrespective of the steel composition. After 1473 K (1200 °C) sintering, the solidified structure

Table I. The Characteristics of Various Powders Used in This Study

Powder	Fe	Fe-1.5Mo	B	Graphite
Purity	>99 pct	>99 pct	>99.9 pct	>95 pct
Composition (wt pct or ppm)				
Ni	—	—	7 ppm	—
Mo	—	1.5 wt pct	—	—
Cu	—	—	10 ppm	—
Mn	—	0.15 wt pct	3 ppm	—
Cr	—	—	10 ppm	—
C	0.003 wt pct	0.01 wt pct	—	—
O	0.08 wt pct	0.15 wt pct	—	—
Particle size (μm)	+212 μm: 0 wt pct +150 μm: 6 wt pct +45 μm: 71 wt pct −45 μm: 23 wt pct	+250 μm: 10 wt pct +150 μm: 10 wt pct +45 μm: 60 wt pct −45 μm: 28 wt pct	−45 μm	−45 μm
Supplier	Höganäs	QMP	ELECMAT	Asbury Carbons
Designation	ASC 100.29	ATOMET 4901	—	1651

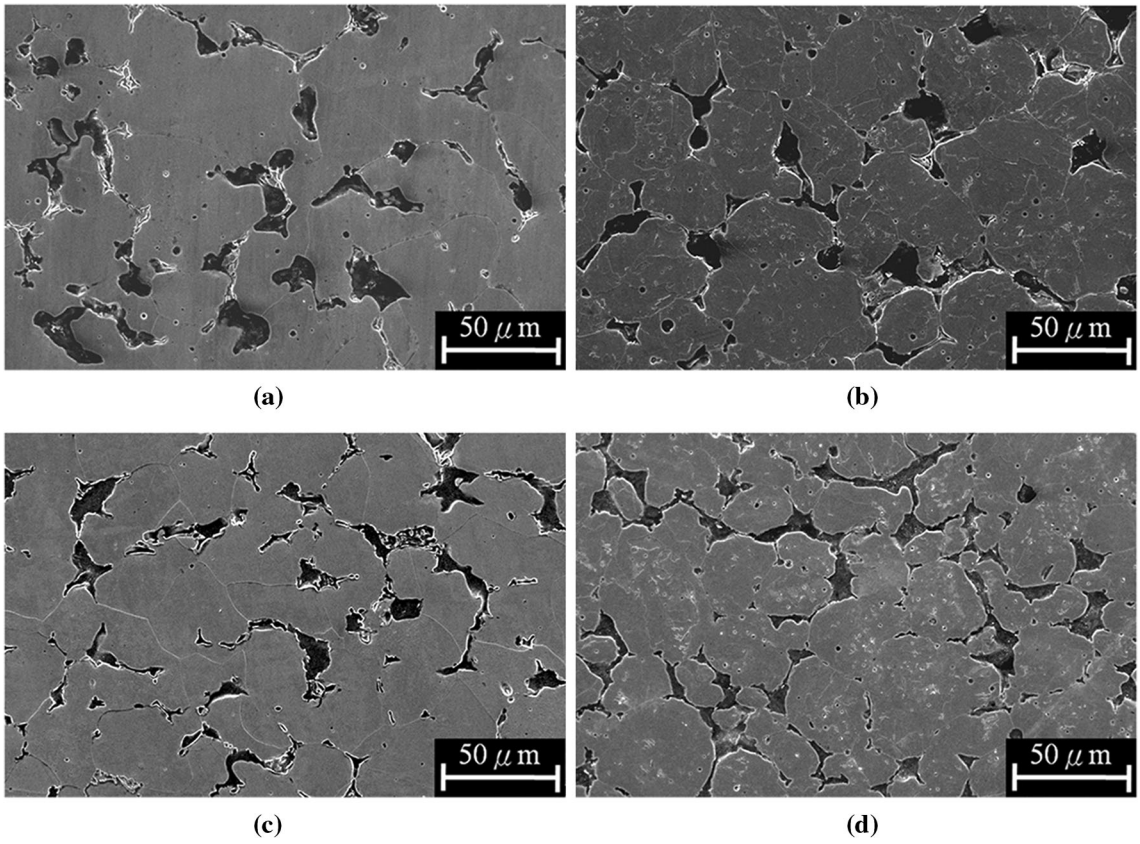

Fig. 1—The microstructures of (*a*) FB, (*b*) FBM, (*c*) FBC, and (*d*) FBMC steels sintered at 1423 K (1150 °C).

and boride could be clearly observed in the FB and FBM steels, as shown in Figures 2(a) and (b). Many spherical secondary pores, which corresponded to the sites of the original boron powder, were also revealed in the microstructure. The microstructures of FB and FBM sintered at 1473 K (1200 °C) were typical of LPS. In contrast, the microstructures of FBC and FBMC steels still retained the characteristics of solid-state sintered steels. The pores were still large and irregular, though solidified structures could be found in these two steels. Moreover, few carbides were dispersed in the ferrite, indicating that the carbon atoms in the original graphite powder had not sufficiently diffused into the base powders even after 1473 K (1200 °C) sintering.

When the sintering temperature was further increased to 1523 K (1250 °C), the densification proceeded and the porosity was further decreased, particularly for the steels with 0.5 wt pct C. Figures 3(c) and (d) clearly indicate large numbers of solidified structures and secondary pores in the FBC and FBMC steels. Furthermore, the microstructures of FBC and FBMC steels at the powder interior consisted of pearlite, implying that most of the carbon atoms in the original graphite powder had diffused into the base powder. These microstructural observations demonstrate that the 0.5 wt pct C addition obviously affected the progress of LPS of B-containing PM steel and that the 1.5 wt pct Mo addition did not, as indicated in Figures 1 through 3. Moreover, the addition of 1.5 wt pct Mo modified the morphology of boride from eutectic to continuous, as shown in Figure 3.

B. *Alloy Distribution*

To identify the alloy distributions in the B-containing PM steels, EPMA was used to map the distributions of boron, molybdenum, carbon, and iron, as shown in Figures 4 through 6. Figure 4 shows the elemental mappings of the FBC steel sintered at 1523 K (1250 °C). The results indicated that boron was mainly concentrated in the solidified area, while carbon was concentrated both in the solidified areas and in the carbides of pearlite. Moreover, rings of ferrite can be clearly observed between the solidified areas and pearlite in Figures 3(c) and 4. Figures 3(c) and 4 show that carbon atoms diffused from the periphery of the iron powder to the center of the powder after 1523 K (1250 °C) sintering. After sintering at that temperature, homogeneous distribution of carbon should be expected. However, the carbon atoms near the powder peripheries could subsequently diffuse to boron-rich areas and participate in the liquid formation, leading to the low carbon content near the liquid phase during LPS. After cooling, the carbon-lean austenite at the powder periphery, carbon-rich austenite in the powder interior, and liquid phase will transform to ferrite, pearlite, and a solidified area, respectively. Ferrite rings were thus generated between the solidified area and the pearlite.

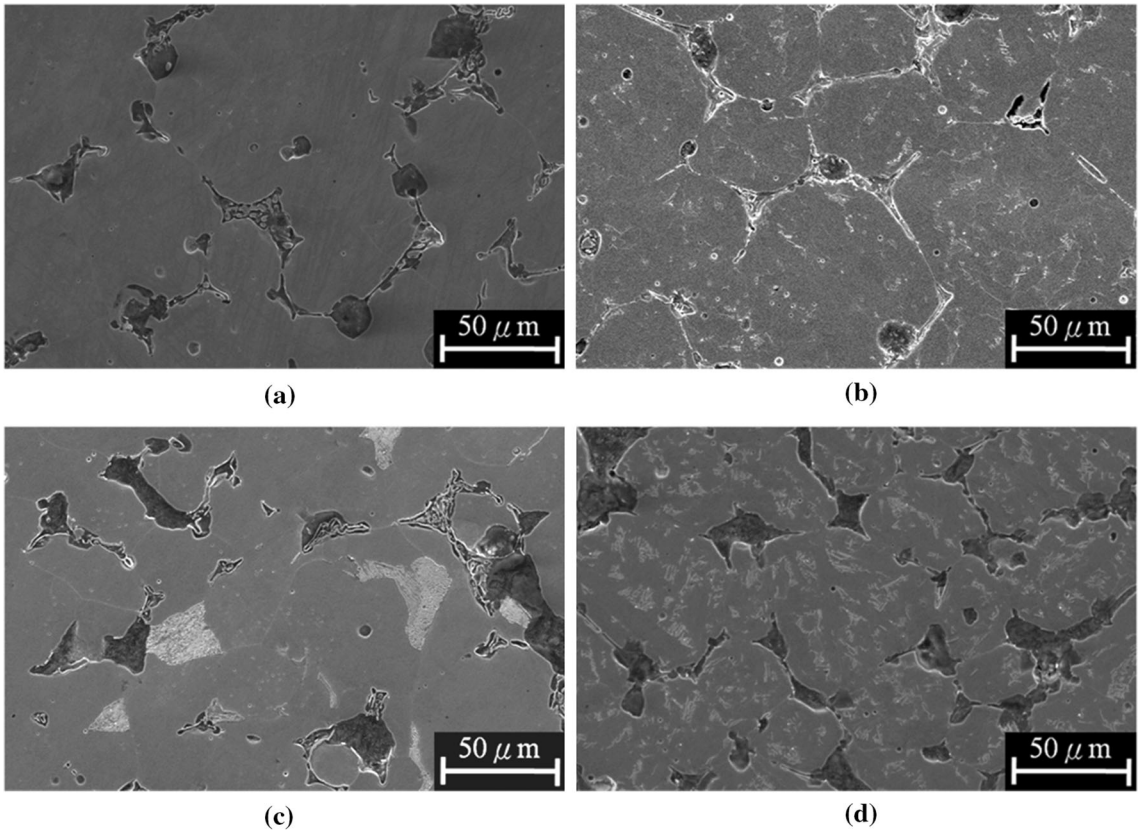

Fig. 2—The microstructures of (*a*) FB, (*b*) FBM, (*c*) FBC, and (*d*) FBMC steels sintered at 1473 K (1200 °C).

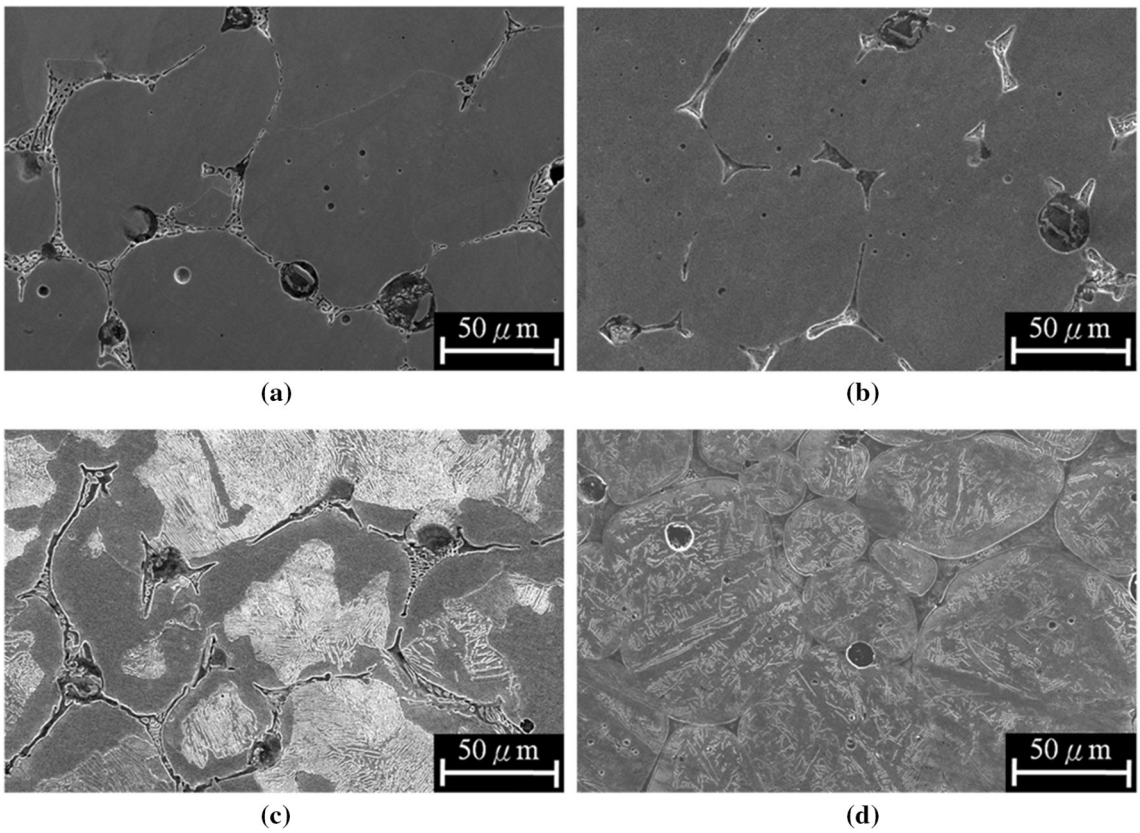

Fig. 3—The microstructures of (*a*) FB, (*b*) FBM, (*c*) FBC, and (*d*) FBMC steels sintered at 1523 K (1250 °C).

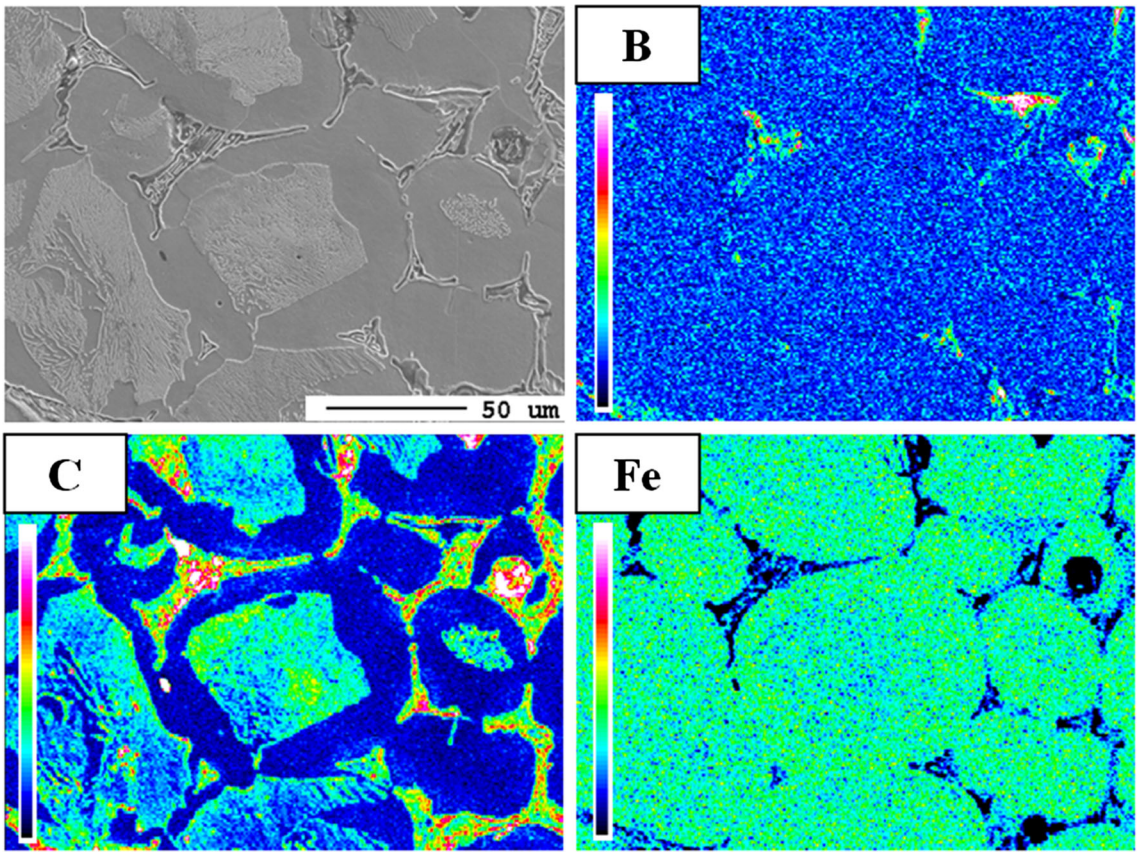

Fig. 4—Elemental mappings of boron, carbon, and iron in the FBC steel sintered at 1523 K (1250 °C).

Figures 5 and 6 show the alloy distributions of FBMC steels sintered at 1473 K and 1523 K (1200 °C and 1250 °C), respectively. These two figures reveal that the distribution of molybdenum corresponded to that of boron. Both molybdenum and boron were concentrated in the solidified areas. However, after 1473 K (1200 °C) sintering, many C-rich areas still remained, indicating that most of the carbon atoms did not diffuse into the base powders, as can be seen in Figures 2(d) and 5. When the sintering temperature was increased to 1523 K (1250 °C), the homogenization of carbon was much improved, as shown in Figure 6. Carbon atoms were mainly concentrated in the solidified areas and in the carbides of pearlite, though a few C-rich areas could also be found. Furthermore, Figures 3(d) and 6 show no ferrite rings in the FBMC steel sintered at 1523 K (1250 °C), indicating that the 1.5 wt pct Mo did in fact change the distribution of carbon in the steel. Molybdenum atoms could reduce the carbon content required for the liquid reaction because molybdenum atoms participated in the liquid formation during LPS. On the other hand, the presence of molybdenum can decrease the chemical potential of carbon in the steel and thus help the homogenization of carbon.[5]

C. *Sintered Density*

Figure 7 presents the sintered densities of the four steels as a function of sintering temperatures. The green densities of various steels are also included in Figure 7. The results indicate that the sintered densities of FB and FBM steels sintered at 1473 K (1200 °C) achieved 7.37 and 7.43 g/cm^3, respectively. The sintered densities slightly increased as the sintering temperature was raised from 1473 K to 1523 K (1200 °C to 1250 °C). The final sintered densities of FB and FBM steels sintered at 1523 K (1250 °C) were 7.39 and 7.49 g/cm^3, respectively. In contrast, the sintered densities of FBC and FBMC steels were merely about 7.31 and 7.26 g/cm^3, respectively, after 1473 K (1200 °C) sintering. The above trend matched the results of the microstructures, as shown in Figure 2. Figure 2 demonstrates that after 1473 K (1200 °C) sintering, sufficient liquid had been generated in the FB and FBM steels for promoting LPS. However, only small amounts of liquid were generated in the FBC and FBMC steels. The pores in the FBC and FBMC steels sintered at 1473 K (1200 °C) were still large and irregular. When the sintering temperature was raised to 1523 K (1250 °C), the sintered densities of FBC (7.48 g/cm^3) and FBMC (7.52 g/cm^3) steels were much improved, even to slightly higher than those of the FB (7.39 g/cm^3) and FBM (7.49 g/cm^3) steels, respectively.

Figure 7 clearly displays the trend of sintered densities of the four steels investigated in this study. However, the final sintered densities of PM steels are also affected by the green densities, in addition to the densification during LPS. To exclude the effect of green density on

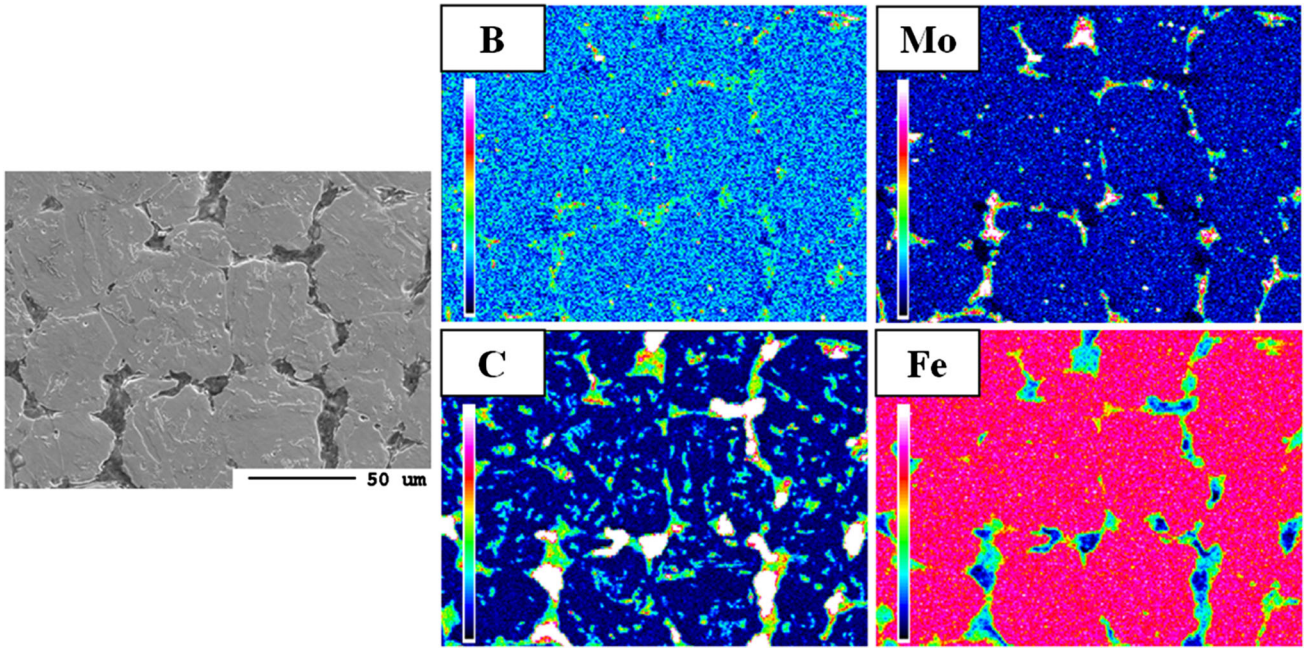

Fig. 5—Elemental mappings of boron, carbon, molybdenum, and iron in the FBMC steel sintered at 1473 K (1200 °C).

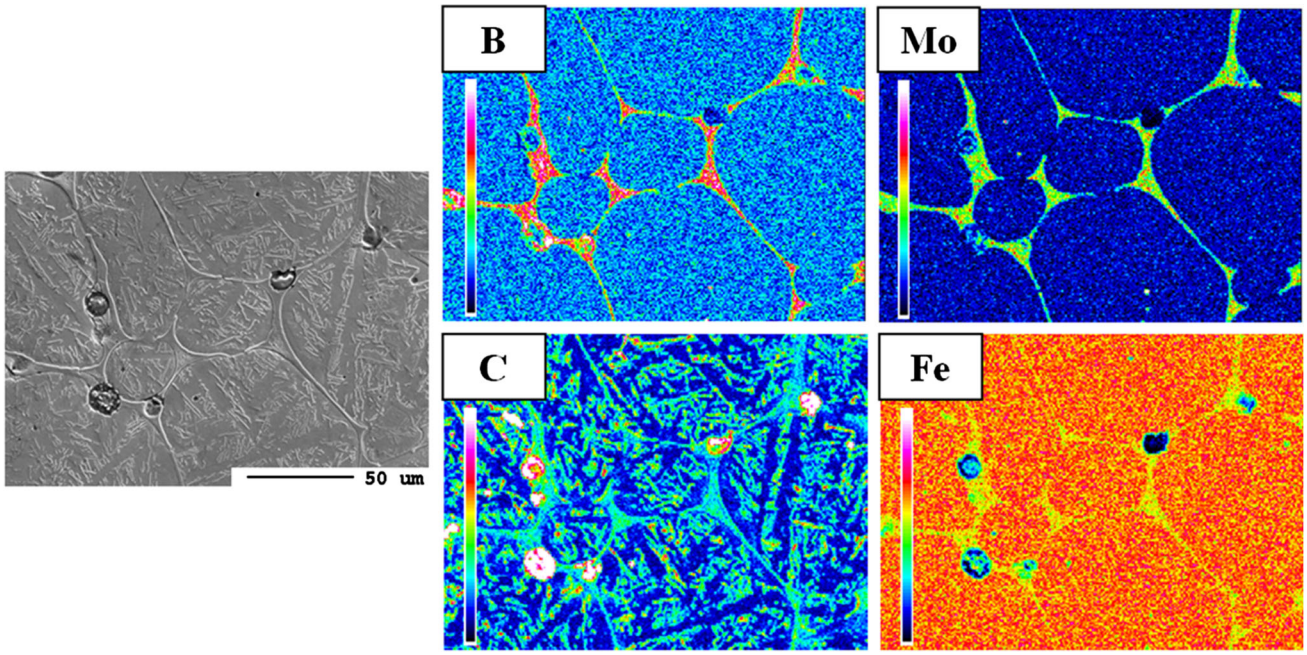

Fig. 6—Elemental mappings of boron, carbon, molybdenum, and iron in the FBMC steel sintered at 1523 K (1250 °C).

densification and sintered density, the differences in the sintered densities after 1523 K (1250 °C) sintering and the green densities of the four steels were also calculated. The increases in the sintered densities of FB, FBM, FBC, and FBMC steels after 1523 K (1250 °C) sintering were 0.33, 0.47, 0.56, and 0.64 g/cm^3, respectively. These findings indicate that adding 0.5 wt pct C or 1.5 wt pct Mo could increase the sintered densities of B-containing PM steels sintered at 1523 K (1250 °C).

D. *Liquid Formation*

To identify why adding 0.5 wt pct C obviously affected the evolution of LPS, the FB and FBC steels

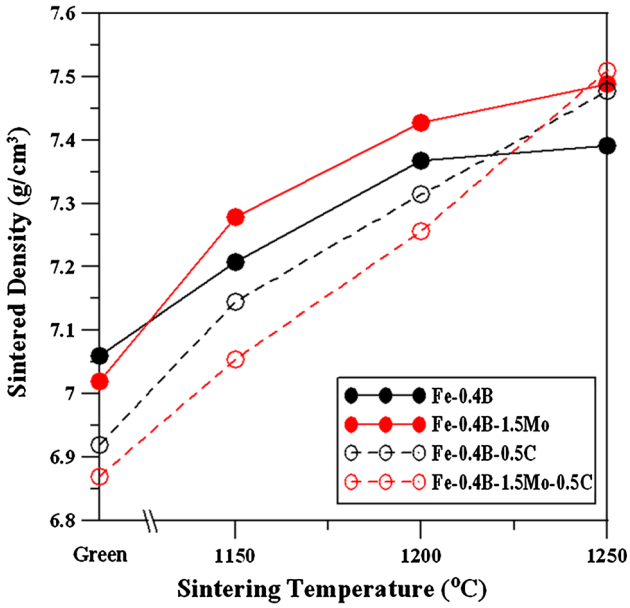

Fig. 7—The sintered densities of four steels as a function of sintering temperature.

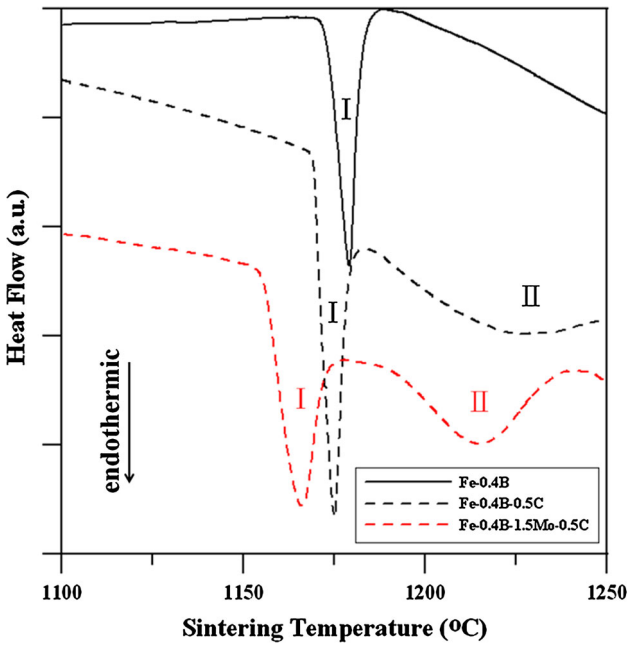

Fig. 8—The heating region of DSC curves for the FB, FBC, and FBMC steels as a function of sintering temperature.

were investigated by DSC, as shown in Figure 8. For the FB steels, there was a single endothermic peak between 1443 K and 1458 K (1170 °C and 1185 °C) for liquid formation, which corresponded to the Fe-B eutectic reaction. However, after 0.5 wt pct C was added, two distinct endothermic peaks for liquid formation were clearly observed. A primary liquid phase formed between the temperatures of 1438 K and 1453 K (1165 °C and 1180 °C). Afterward, a secondary liquid phase was generated between 1453 K and 1523 K (1180 °C and 1250 °C), intensifying at about 1498 K

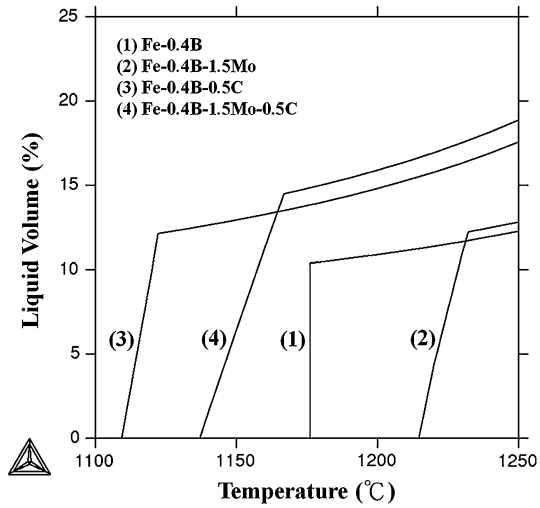

Fig. 9—The liquid volumes of four steels simulated by Thermo-Calc program as a function of temperature.

(1225 °C). These results clearly indicate that adding carbon to the FB steels changed the liquid formation and thus the progress of LPS. When the FBC steel was sintered at 1523 K (1250 °C), the secondary liquid phase was activated, the densification was better than in the FB steels. The DSC curve of the FBMC steel, included in Figure 8, also shows that adding 1.5 wt pct Mo to FBC steel could decrease the temperature for liquid formation. However, like in the FBC steel, two distinct regions for liquid formation were also observed in the FBMC steel.

Momeni *et al.*[21] also used thermal analyses to investigate LPS of Fe-0.88B-0.8C and found that the sintering atmosphere obviously affects the temperature of liquid formation. These authors reported that a large endothermic peak is generated in the temperature ranges of 1434 K to 1450 K (1161 °C to 1177 °C) and 1403 K to 1430 K (1130 °C to 1157 °C) in atmospheres of N_2 and Ar, respectively. The temperatures for liquid formation in N_2 and Ar are close to the binary Fe-B and ternary Fe-B-C eutectic reaction temperatures, respectively. However, during the sintering of Fe-0.88B-0.8C in Ar, Momeni *et al.*[21] observed only one endothermic peak, which is inconsistent with the finding in Figure 8. This discrepancy could be due to the differences in the boron source (Fe-18 pct B master alloy powder) and chemical composition used in their study.

E. *Liquid Volume*

The effects of 0.5 wt pct C addition on the formation of the secondary liquid phase were clarified in the previous section. To evaluate the amount of liquid phase that formed during LPS, the percentage of liquid volume in the four steels as a function of temperature was simulated by Thermo-Calc software, as demonstrated in Figure 9. It was clear that the simulated temperatures for liquid formation in various steels were not identical to those obtained from DSC results, except for those of the FB steel, as can be seen from comparing

Figures 8 and 9. This discrepancy can be explained in detail as follows.

The four steels were produced by mixing Fe-based powders, elemental boron powder, and graphite powder, followed by compaction and sintering. These steels were in a non-equilibrium state during heating. To achieve an equilibrium state, the separate elements diffused in each steel. However, since thermodynamic simulation software is normally used to calculate various properties in an equilibrium state, the experimental results obtained for a non-equilibrium state did not coincide with the ones simulated with Thermo-Calc software. Furthermore, the microstructural observations in Figures 1 through 3 clearly indicate that the states of the four steels sintered at 1423 K and 1473 K (1150 °C and 1200 °C) still deviated greatly from the equilibrium state. However, after 1523 K (1250 °C) sintering, the four steels were close to the equilibrium state, as shown in Figures 3 and 6. The liquid volumes at 1523 K (1250 °C) were thus indicative of the effects of the various elements on LPS.

The liquid volumes in the FB, FBM, FBC, and FBMC steels sintered at 1523 K (1250 °C) were 12.1, 12.8, 17.5, 18.9 vol pct, respectively. Adding 1.5 wt pct Mo to FB and FBC steels increased the liquid volume by about 1 vol pct. However, adding 0.5 wt pct C to FB and FBM steels increased the liquid volume by about 5 to 6 vol pct. Altogether, the thermodynamic simulations (Figure 9), the resulting sintered densities (Figure 7), and the thermal analyses (Figure 8) clearly demonstrated that adding 0.5 wt pct C or 1.5 wt pct Mo improved the LPS densification and the sintered densities after 1523 K (1250 °C) sintering, particularly 0.5 wt pct C. The combination of 0.5 wt pct C and 1.5 wt pct Mo resulted in better densification than either 0.5 wt pct C or 1.5 wt pct Mo alone. In conclusion, the addition of 0.5 wt pct C in B-containing PM steels facilitated the formation of a secondary liquid phase and a higher liquid volume, resulting in superior LPS densification.

IV. CONCLUSIONS

This study clarified the influences of carbon and molybdenum on the microstructure, alloy distribution, sintered density, liquid formation, and liquid volume of B-containing PM steels during LPS. The findings are summarized as follows:

1. After 1473 K (1200 °C) sintering, the FB and FBM steels have microstructures typical of LPS. In the FBC and FBMC steels, however, if 0.5 wt pct C is added, the typical microstructures produced by solid-state sintering are still found. When the sintering temperature is increased to 1523 K (1250 °C), LPS is activated, and the sintered densities of FBC and FBMC steels are much improved.
2. In the four steels investigated in this study, the distribution of molybdenum corresponded to that of boron, and these two elements predominantly segregated in the solidified areas. In the steels with carbon, carbon atoms are concentrated in not only the carbides but also the borides.
3. After 1523 K (1250 °C) sintering, the sintered densities of FB, FBM, FBC, and FBMC steels increases to 0.33, 0.47, 0.56, and 0.64 g/cm^3, respectively. These results demonstrate that adding 0.5 wt pct C or 1.5 wt pct Mo can increase the sintered density.
4. During sintering of FB steel, only one endothermic peak is observed. The added carbon obviously modifies the progress of LPS. With the addition of 0.5 wt pct C, liquid is generated in two distinct regions, and the secondary liquid phase improves the densification.
5. Thermodynamic simulation showed that, at 1523 K (1250 °C), the liquid volumes in the FB, FBM, FBC, and FBMC steels are 12.1, 12.8, 17.5, 18.9 vol pct, respectively. Adding 0.5 wt pct C to B-containing PM steels facilitates the formation of a secondary liquid phase and a higher liquid volume, resulting in superior LPS densification.

ACKNOWLEDGMENTS

The author thanks the Ministry of Science and Technology of the Republic of China for the support under contract number MOST 103-2221-E-027-132. My gratitude is also extended to QMP and Höganäs AB for providing the base powders and Yu-Chi Fan for the preparations of specimens investigated in this study.

REFERENCES

1. M. Campos, J. Sicre-Artalejo, J.J. Munoz, and J.M. Torralba: *Metall. Mater. Trans. A*, 2010, vol. 41A, pp. 1847–54.
2. M. Gauthier, S. Metcalfe, S. Pelletier, and T.F. Stephenson: *Powder Metall.*, 2011, vol. 54, pp. 628–35.
3. K.S. Moghaddam and N. Solimanjad: *Powder Metall.*, 2013, vol. 56, pp. 245–50.
4. F. Bernier, P. Plamondon, J.P. Baïlon, and G. L'Espèrance: *Powder Metall.*, 2011, vol. 54, pp. 559–65.
5. M.W. Wu, K.S. Hwang, and H.S. Huang: *Metall. Mater. Trans. A*, 2007, vol. 38A, pp. 1598–1607.
6. M.W. Wu, L.C. Tsao, G.J. Shu, and B.H. Lin: *Mater. Sci. Eng. A*, 2012, vol. 538, pp. 135–44.
7. M.W. Wu, G.J. Shu, S.Y. Chang, and B.H. Lin: *Metall. Mater. Trans. A*, 2014, vol. 45A, pp. 3866–75.
8. J.M. Torralba, A. Navarro, and M. Campos: *Mater. Sci. Eng. A*, 2013, vol. 573, pp. 253–56.
9. R. Oro, M. Campos, J.M. Torralba, and C. Capdevila: *Powder Metall.*, 2012, vol. 55, pp. 294–301.
10. B.A. Gething, D.F. Heaney, D.A. Koss, and T.J. Mueller: *Mater. Sci. Eng. A*, 2005, vol. 390, pp. 19–26.
11. H. Danninger, C. Xu, G. Khatibi, B. Weiss, and B. Lindqvist: *Powder Metall.*, 2012, vol. 55, pp. 378–87.
12. X. Denga, G. Piotrowski, N. Chawla, and K.S. Narasimhan: *Mater. Sci. Eng. A*, 2008, vol. 491, pp. 19–27.
13. T.M. Puscas, M. Signorini, A. Molinari, and G. Straffelini: *Mater. Charact.*, 2003, vol. 50, pp. 1–10.
14. R.M. German, K.S. Hwang, and D.S. Madan: *Powder Metall. Int.*, 1987, vol. 19, pp. 15–18.
15. E. Dudrová, M. Selecká, R. Bureś, and M. Kabátová: *ISIJ Int.*, 1997, vol. 37, pp. 59–64.
16. M. Selecká, A. Šalak, and H. Danninger: *J. Mater. Process. Technol.*, 2003, vols. 143–144, pp. 910–15.
17. M. Sarasola, T.G. Acebo, and F. Castro: *Acta Mater.*, 2004, vol. 52, pp. 4615–22.

18. M. Sarasola, T.G. Acebo, and F. Castro: *Powder Metall.*, 2005, vol. 48, pp. 59–67.
19. A. Molinari, T. Pieczonka, J. Kazior, S. Gialanella, and G. Straffelini: *Metall. Mater. Trans. A*, 2000, vol. 31A, pp. 1497–1506.
20. J.K. Baczewska and M. Rosso: *Powder Metall. Prog.*, 2006, vol. 6, pp. 11–19.
21. M. Momeni, C. Gierl, H. Danninger, and A. Avakemian: *Powder Metall.*, 2012, vol. 55, pp. 54–64.
22. J. Liu, A. Cardamone, T. Potter, R.M. German, and F.J. Semel: *Powder Metall.*, 2000, vol. 43, pp. 57–61.
23. Z. Xiu, A. Salwen, X. Qin, F. He, and X. Sun: *Powder Metall.*, 2003, vol. 46, pp. 171–74.
24. H.Ö. Gulsoy: *Scripta Mater.*, 2005, vol. 52, pp. 187–92.
25. T.B. Sercombe: *Mater. Sci. Eng. A*, 2003, vol. 363, pp. 242–52.
26. T.B. Sercombe and G.B. Schaffer: *Mater. Sci. Eng. A*, 2010, vol. 528, pp. 751–55.
27. G. Cui and Z. Kou: *J. Alloys Compd.*, 2014, vol. 586, pp. 699–702.
28. R.L. Lawcock and T.J. Davies: *Powder Metall.*, 1990, vol. 33, pp. 147–50.
29. C.T. Huang and K.S. Hwang: *Powder Metall.*, 1996, vol. 39, pp. 119–23.
30. A. Molinari, G. Straffelini, V. Fontanari, and R. Canteri: *Powder Metall.*, 1992, vol. 35, pp. 285–91.
31. G. Straffelini, V. Fontanari, A. Molinari, and B. Tesi: *Powder Metall.*, 1993, vol. 36, pp. 135–41.
32. K. Zhu, C. Oberbillig, C. Musik, D. Loison, and T. Iung: *Mater. Sci. Eng. A*, 2011, vol. 528, pp. 4222–31.
33. B. Hwang, D.W. Suh, and S.J. Kim: *Scripta Mater.*, 2011, vol. 64, pp. 1118–20.